Single-spin asymmetry of J/ production in p+p, p+Al, and p+Au collisions with transversely polarized proton beams at sNN=200 GeV

Single-spin asymmetry of J/ψ production in $p+p$, $p+$Al, and $p+$Au collisions with transversely polarized proton beams at $\sqrt{s_{NN}} = 200$ GeV

C. Aidala,[39] Y. Akiba,[50,51,†] M. Alfred,[22] V. Andrieux,[39] N. Apadula,[27] H. Asano,[32,50] B. Azmoun,[7] V. Babintsev,[23] A. Bagoly,[16] N. S. Bandara,[38] K. N. Barish,[8] S. Bathe,[5,51] A. Bazilevsky,[7] M. Beaumier,[8] R. Belmont,[12] A. Berdnikov,[53] Y. Berdnikov,[53] D. S. Blau,[31,42] M. Boer,[34] J. S. Bok,[44] M. L. Brooks,[34] J. Bryslawskyj,[5,8] V. Bumazhnov,[23] S. Campbell,[13] V. Canoa Roman,[56] R. Cervantes,[56] C. Y. Chi,[13] M. Chiu,[7] I. J. Choi,[24] J. B. Choi,[10,*] Z. Citron,[61] M. Connors,[20,51] N. Cronin,[56] M. Csanád,[16] T. Csörgő,[17,62] T. W. Danley,[45] M. S. Daugherity,[1] G. David,[7,56] K. DeBlasio,[43] K. Dehmelt,[56] A. Denisov,[23] A. Deshpande,[51,56] E. J. Desmond,[7] A. Dion,[56] D. Dixit,[56] J. H. Do,[63] A. Drees,[56] K. A. Drees,[6] J. M. Durham,[34] A. Durum,[23] A. Enokizono,[50,52] H. En'yo,[50] S. Esumi,[59] B. Fadem,[40] W. Fan,[56] N. Feege,[56] D. E. Fields,[43] M. Finger,[9] M. Finger, Jr.,[9] S. L. Fokin,[31] J. E. Frantz,[45] A. Franz,[7] A. D. Frawley,[19] Y. Fukuda,[59] C. Gal,[56] P. Gallus,[14] P. Garg,[3,56] H. Ge,[56] F. Giordano,[24] Y. Goto,[50,51] N. Grau,[2] S. V. Greene,[60] M. Grosse Perdekamp,[24] T. Gunji,[11] H. Guragain,[20] T. Hachiya,[50,51] J. S. Haggerty,[7] K. I. Hahn,[18] H. Hamagaki,[11] H. F. Hamilton,[1] S. Y. Han,[18] J. Hanks,[56] S. Hasegawa,[28] T. O. S. Haseler,[20] X. He,[20] T. K. Hemmick,[56] J. C. Hill,[27] K. Hill,[12] A. Hodges,[20] R. S. Hollis,[8] K. Homma,[21] B. Hong,[30] T. Hoshino,[21] N. Hotvedt,[27] J. Huang,[7] S. Huang,[60] K. Imai,[28] M. Inaba,[59] A. Iordanova,[8] D. Isenhower,[1] D. Ivanishchev,[49] B. V. Jacak,[56] M. Jezghani,[20] Z. Ji,[56] X. Jiang,[34] B. M. Johnson,[7,20] D. Jouan,[47] D. S. Jumper,[24] J. H. Kang,[63] D. Kapukchyan,[8] S. Karthas,[56] D. Kawall,[38] A. V. Kazantsev,[31] V. Khachatryan,[56] A. Khanzadeev,[49] C. Kim,[8,30] E.-J. Kim,[10] M. Kim,[54] D. Kincses,[16] E. Kistenev,[7] J. Klatsky,[19] P. Kline,[56] T. Koblesky,[12] D. Kotov,[49,53] S. Kudo,[59] K. Kurita,[52] Y. Kwon,[63] J. G. Lajoie,[27] A. Lebedev,[27] S. Lee,[63] S. H. Lee,[27,56] M. J. Leitch,[34] Y. H. Leung,[56] N. A. Lewis,[39] X. Li,[34] S. H. Lim,[34,63] M. X. Liu,[34] V.-R. Loggins,[24] S. Lökös,[16,17] K. Lovasz,[15] D. Lynch,[7] T. Majoros,[15] Y. I. Makdisi,[6] M. Makek,[64] V. I. Manko,[31] E. Mannel,[7] M. McCumber,[34] P. L. McGaughey,[34] D. McGlinchey,[12,34] C. McKinney,[24] M. Mendoza,[8] A. C. Mignerey,[37] D. E. Mihalik,[56] A. Milov,[61] D. K. Mishra,[4] J. T. Mitchell,[7] G. Mitsuka,[51] S. Miyasaka,[50,58] S. Mizuno,[50,59] P. Montuenga,[24] T. Moon,[63] D. P. Morrison,[7] S. I. Morrow,[60] T. Murakami,[32,50] J. Murata,[50,52] K. Nagai,[58] K. Nagashima,[21] T. Nagashima,[52] J. L. Nagle,[12] M. I. Nagy,[16] I. Nakagawa,[50,51] K. Nakano,[50,58] C. Nattrass,[57] T. Niida,[59] R. Nouicer,[7,51] T. Novák,[17,62] N. Novitzky,[56] A. S. Nyanin,[31] E. O'Brien,[7] C. A. Ogilvie,[27] J. D. Orjuela Koop,[12] J. D. Osborn,[39] A. Oskarsson,[35] G. J. Ottino,[43] K. Ozawa,[29,59] V. Pantuev,[25] V. Papavassiliou,[44] J. S. Park,[54] S. Park,[50,54,56] S. F. Pate,[44] M. Patel,[27] W. Peng,[60] D. V. Perepelitsa,[7,12] G. D. N. Perera,[44] D. Yu. Peressounko,[31] C. E. PerezLara,[56] J. Perry,[27] R. Petti,[7] M. Phipps,[7,24] C. Pinkenburg,[7] R. P. Pisani,[7] M. L. Purschke,[7] P. V. Radzevich,[53] K. F. Read,[46,57] D. Reynolds,[55] V. Riabov,[42,49] Y. Riabov,[49,53] D. Richford,[5] T. Rinn,[27] S. D. Rolnick,[8] M. Rosati,[27] Z. Rowan,[5] J. Runchey,[27] A. S. Safonov,[53] T. Sakaguchi,[7] H. Sako,[28] V. Samsonov,[42,49] M. Sarsour,[20] S. Sato,[28] B. Schaefer,[60] B. K. Schmoll,[57] K. Sedgwick,[8] R. Seidl,[50,51] A. Sen,[27,57] R. Seto,[8] A. Sexton,[37] D. Sharma,[56] I. Shein,[23] T.-A. Shibata,[50,58] K. Shigaki,[21] M. Shimomura,[27,41] T. Shioya,[59] P. Shukla,[4] A. Sickles,[24] C. L. Silva,[34] D. Silvermyr,[35] B. K. Singh,[3] C. P. Singh,[3] V. Singh,[3] M. J. Skoby,[39] M. Slunečka,[9] M. Snowball,[34] R. A. Soltz,[33] W. E. Sondheim,[34] S. P. Sorensen,[57] I. V. Sourikova,[7] P. W. Stankus,[46] S. P. Stoll,[7] T. Sugitate,[21] A. Sukhanov,[7] T. Sumita,[50] J. Sun,[56] Z. Sun,[15] J. Sziklai,[62] K. Tanida,[28,51,54] M. J. Tannenbaum,[7] S. Tarafdar,[60,61] A. Taranenko,[42,55] G. Tarnai,[15] R. Tieulent,[20,36] A. Timilsina,[27] T. Todoroki,[59] M. Tomášek,[14] C. L. Towell,[1] R. S. Towell,[1] I. Tserruya,[61] Y. Ueda,[21] B. Ujvari,[15] H. W. van Hecke,[34] J. Velkovska,[60] M. Virius,[14] V. Vrba,[14,26] N. Vukman,[64] X. R. Wang,[44,51] Y. S. Watanabe,[11] C. P. Wong,[20] C. L. Woody,[7] C. Xu,[44] Q. Xu,[60] L. Xue,[20] S. Yalcin,[56] Y. L. Yamaguchi,[51,56] H. Yamamoto,[59] A. Yanovich,[23] J. H. Yoo,[30] I. Yoon,[54] H. Yu,[44,48] I. E. Yushmanov,[31] W. A. Zajc,[13] A. Zelenski,[6] S. Zharko,[53] and L. Zou[8]

(PHENIX Collaboration)

[1]*Abilene Christian University, Abilene, Texas 79699, USA*
[2]*Department of Physics, Augustana University, Sioux Falls, South Dakota 57197, USA*
[3]*Department of Physics, Banaras Hindu University, Varanasi 221005, India*
[4]*Bhabha Atomic Research Centre, Bombay 400 085, India*
[5]*Baruch College, City University of New York, New York, New York 10010, USA*
[6]*Collider-Accelerator Department, Brookhaven National Laboratory, Upton, New York 11973-5000, USA*
[7]*Physics Department, Brookhaven National Laboratory, Upton, New York 11973-5000, USA*
[8]*University of California-Riverside, Riverside, California 92521, USA*
[9]*Charles University, Ovocný trh 5, Praha 1, 116 36, Prague, Czech Republic*
[10]*Chonbuk National University, Jeonju, 561-756, Korea*

[11]*Center for Nuclear Study, Graduate School of Science, University of Tokyo,*
7-3-1 Hongo, Bunkyo, Tokyo 113-0033, Japan
[12]*University of Colorado, Boulder, Colorado 80309, USA*
[13]*Columbia University, New York, New York 10027*
and Nevis Laboratories, Irvington, New York 10533, USA
[14]*Czech Technical University, Zikova 4, 166 36 Prague 6, Czech Republic*
[15]*Debrecen University, H-4010 Debrecen, Egyetem tér 1, Hungary*
[16]*ELTE, Eötvös Loránd University, H-1117 Budapest, Pázmány P. s. 1/A, Hungary*
[17]*Eszterházy Károly University, Károly Róbert Campus, H-3200 Gyöngyös, Mátrai út 36, Hungary*
[18]*Ewha Womans University, Seoul 120-750, Korea*
[19]*Florida State University, Tallahassee, Florida 32306, USA*
[20]*Georgia State University, Atlanta, Georgia 30303, USA*
[21]*Hiroshima University, Kagamiyama, Higashi-Hiroshima 739-8526, Japan*
[22]*Department of Physics and Astronomy, Howard University, Washington, D.C. 20059, USA*
[23]*IHEP Protvino, State Research Center of Russian Federation, Institute for High Energy Physics,*
Protvino, 142281, Russia
[24]*University of Illinois at Urbana-Champaign, Urbana, Illinois 61801, USA*
[25]*Institute for Nuclear Research of the Russian Academy of Sciences,*
prospekt 60-letiya Oktyabrya 7a, Moscow 117312, Russia
[26]*Institute of Physics, Academy of Sciences of the Czech Republic,*
Na Slovance 2, 182 21 Prague 8, Czech Republic
[27]*Iowa State University, Ames, Iowa 50011, USA*
[28]*Advanced Science Research Center, Japan Atomic Energy Agency,*
2-4 Shirakata Shirane, Tokai-mura, Naka-gun, Ibaraki-ken 319-1195, Japan
[29]*KEK, High Energy Accelerator Research Organization, Tsukuba, Ibaraki 305-0801, Japan*
[30]*Korea University, Seoul, 136-701, Korea*
[31]*National Research Center "Kurchatov Institute", Moscow, 123098 Russia*
[32]*Kyoto University, Kyoto 606-8502, Japan*
[33]*Lawrence Livermore National Laboratory, Livermore, California 94550, USA*
[34]*Los Alamos National Laboratory, Los Alamos, New Mexico 87545, USA*
[35]*Department of Physics, Lund University, Box 118, SE-221 00 Lund, Sweden*
[36]*IPNL, CNRS/IN2P3, Univ Lyon, Université Lyon 1, F-69622, Villeurbanne, France*
[37]*University of Maryland, College Park, Maryland 20742, USA*
[38]*Department of Physics, University of Massachusetts, Amherst, Massachusetts 01003-9337, USA*
[39]*Department of Physics, University of Michigan, Ann Arbor, Michigan 48109-1040, USA*
[40]*Muhlenberg College, Allentown, Pennsylvania 18104-5586, USA*
[41]*Nara Women's University, Kita-uoya Nishi-machi Nara 630-8506, Japan*
[42]*National Research Nuclear University, MEPhI, Moscow Engineering Physics Institute,*
Moscow, 115409, Russia
[43]*University of New Mexico, Albuquerque, New Mexico 87131, USA*
[44]*New Mexico State University, Las Cruces, New Mexico 88003, USA*
[45]*Department of Physics and Astronomy, Ohio University, Athens, Ohio 45701, USA*
[46]*Oak Ridge National Laboratory, Oak Ridge, Tennessee 37831, USA*
[47]*IPN-Orsay, Univ. Paris-Sud, CNRS/IN2P3, Université Paris-Saclay, BP1, F-91406, Orsay, France*
[48]*Peking University, Beijing 100871, People's Republic of China*
[49]*PNPI, Petersburg Nuclear Physics Institute, Gatchina, Leningrad region, 188300, Russia*
[50]*RIKEN Nishina Center for Accelerator-Based Science, Wako, Saitama 351-0198, Japan*
[51]*RIKEN BNL Research Center, Brookhaven National Laboratory, Upton, New York 11973-5000, USA*
[52]*Physics Department, Rikkyo University, 3-34-1 Nishi-Ikebukuro, Toshima, Tokyo 171-8501, Japan*
[53]*Saint Petersburg State Polytechnic University, St. Petersburg, 195251 Russia*
[54]*Department of Physics and Astronomy, Seoul National University, Seoul 151-742, Korea*
[55]*Chemistry Department, Stony Brook University, SUNY, Stony Brook, New York 11794-3400, USA*
[56]*Department of Physics and Astronomy, Stony Brook University, SUNY,*
Stony Brook, New York 11794-3800, USA
[57]*University of Tennessee, Knoxville, Tennessee 37996, USA*
[58]*Department of Physics, Tokyo Institute of Technology, Oh-okayama, Meguro, Tokyo 152-8551, Japan*
[59]*Tomonaga Center for the History of the Universe, University of Tsukuba, Tsukuba, Ibaraki 305, Japan*
[60]*Vanderbilt University, Nashville, Tennessee 37235, USA*
[61]*Weizmann Institute, Rehovot 76100, Israel*

^{62}*Institute for Particle and Nuclear Physics, Wigner Research Centre for Physics,*
Hungarian Academy of Sciences (Wigner RCP, RMKI)
H-1525 Budapest 114, POBox 49, Budapest, Hungary
^{63}*Yonsei University, IPAP, Seoul 120-749, Korea*
^{64}*Department of Physics, Faculty of Science, University of Zagreb,*
Bijenička c. 32 HR-10002 Zagreb, Croatia

We report the transverse single-spin asymmetries of J/ψ production at forward and backward rapidity, $1.2 < |y| < 2.2$, as a function of J/ψ transverse momentum (p_T) and Feynman-x (x_F). The data analyzed were recorded by the PHENIX experiment at the Relativistic Heavy Ion Collider in 2015 from $p + p$, $p + $ Al, and $p + $ Au collisions with transversely polarized proton beams at $\sqrt{s_{NN}} = 200$ GeV. At this collision energy, single-spin asymmetries for heavy-flavor particle production of $p + p$ collisions provide access to the spin-dependent gluon distribution and higher-twist correlation functions inside the nucleon, such as the gluon Qiu-Sterman and trigluon correlation functions. Proton + nucleus collisions offer an excellent opportunity to study nuclear effects on the correlation functions. The data indicate a positive asymmetry at the two-standard-deviation level in the $p + p$ data for 2 GeV/$c < p_T < 10$ GeV/c at backward rapidity and negative asymmetries at the two-standard-deviation level in the $p + $ Au data for $p_T < 2$ GeV/c at both forward and backward rapidity, while in $p + $ Al collisions the asymmetries are consistent with zero within the range of experimental uncertainties.

I. INTRODUCTION

In polarized $p + p$ collisions, the transverse single spin asymmetry (TSSA), A_N, is defined as the amplitude of the azimuthal angular modulation of the outgoing particle's scattering cross section with respect to the transverse spin direction of the polarized proton. Early theoretical predictions which were purely based on perturbative calculations showed that the TSSA should be inversely proportional to the hard scale of the scattering [1], and if applied to the reactions at energies accessible at the Relativistic Heavy Ion Collider (RHIC), the asymmetry would be very small, of order 10^{-4}. However, the experimental asymmetries of light-flavored hadrons turned out to be much larger, $A_N = O(10^{-1})$ [2,3].

To explain what has been observed in experiments, several theoretical frameworks [4–8] were developed in the 1990s. In the collinear factorization framework, contributions from multiparton correlations to the transverse-spin-dependent cross section were introduced through three types of spin-momentum correlations: (1) twist-3 correlation functions of a polarized hadron $\phi^{(3)}_{a/A}(x_1, x_2, \vec{s}_\perp)$ convolved with leading-twist correlation functions of an unpolarized hadron $\phi_{b/B}(x')$ and with leading-twist parton fragmentation functions $D_{c\to C}(z)$, (2) transversity parton distribution functions $\delta q_{a/A}(x, \vec{s}_\perp)$ convolved with twist-3 correlation functions of an unpolarized hadron $\phi^{(3)}_{b/B}(x'_1, x'_2)$ and leading-twist parton fragmentation functions $D_{c\to C}(z)$, and (3) transversity parton distribution functions $\delta q_{a/A}(x, \vec{s}_\perp)$ convolved with leading-twist correlation functions of an unpolarized hadron $\phi_{b/B}(x')$ and with twist-3 fragmentation functions $D^{(3)}_{c\to C}(z_1, z_2)$ [9],

$$
\begin{aligned}
A_N \propto &\sum_{abc} \phi^{(3)}_{a/A}(x_1, x_2, \vec{s}_\perp) \otimes \phi_{b/B}(x') \otimes \hat{\sigma} \otimes D_{c\to C}(z) \\
&+ \sum_{abc} \delta q_{a/A}(x, \vec{s}_\perp) \otimes \phi^{(3)}_{b/B}(x'_1, x'_2) \otimes \hat{\sigma}' \otimes D_{c\to C}(z) \\
&+ \sum_{abc} \delta q_{a/A}(x, \vec{s}_\perp) \otimes \phi_{b/B}(x') \otimes \hat{\sigma}'' \otimes D^{(3)}_{c\to C}(z_1, z_2).
\end{aligned}
\tag{1}
$$

In this notation, a/A means the distribution of parton a in hadron A, b/B means the distribution of parton b in hadron B and $c \to C$ means the fragmentation of parton c into hadron C. Additionally, x is the Bjorken parton momentum fraction of the incoming hadron; z is the fraction of the outgoing partonic momentum carried by the detected hadron; $\vec{s}_\perp$ is the transverse spin of the incoming hadron; $\hat{\sigma}$, $\hat{\sigma}'$, and $\hat{\sigma}''$ are the partonic hard-scattering cross sections of a process where a higher twist is associated with the incoming polarized or unpolarized hadron, or outgoing partons, respectively. Nonzero values for $\phi^{(3)}_{a/A}(x_1, x_2, \vec{s}_\perp)$

---

and $D_{c \to C}^{(3)}(z_1, z_2)$ in Eq. (1) account for the large A_N observed in experiment, where $\phi_{a/A}^{(3)}(x_1, x_2, \vec{s}_\perp)$ corresponds to initial-state effects [8] and $D_{c \to C}^{(3)}(z_1, z_2)$ to final-state effects [10]. Initial-state effects are described by the twist-3 three-parton correlation functions $\phi_{a/A}^{(3)}(x_1, x_2, \vec{s}_\perp)$ and $\phi_{b/B}^{(3)}(x_1', x_2')$ which measure the quantum interference between two scattering amplitudes of the incoming hadron [11], while final-state effects are related to twist-3 fragmentation functions $D_{c \to C}^{(3)}(z_1, z_2)$ which describe the process in which the outgoing parton fragments into a final-state hadron [11]. At RHIC energies, heavy quark production, such as J/ψ production, is dominated by gluon-gluon interactions. Because the gluon transversity distribution does not exist, the second and third terms of Eq. (1) are zero. This means that the heavy flavor A_N is free from final-state effects and is sensitive to initial-state effects, such as the gluon Qiu-Sterman and trigluon correlations which correspond to the factor $\phi_{a/A}^{(3)}(x_1, x_2, \vec{s}_\perp)$ in Eq. (1) [12].

In the case of high energy hadronic collisions, a non-vanishing SSA is generated by a parton-level spin flip and a phase difference between the scattering amplitude and the corresponding complex conjugate. In the context of the quantum chromodynamic (QCD) collinear-factorization framework, the parton-level spin flip is generated by the interference between the active single parton and a two-parton composite state of the scattering amplitude. On the other hand, the phase difference is achieved by the interference between the real and imaginary part of the partonic scattering amplitude [8,9,13]. For the Qiu-Sterman correlation, the quantum interference is between a quark state of momentum fraction x and a quark-gluon composite state with the same momentum fraction where either the gluon or quark carries the total momentum of the quark-gluon composite state [14]. In the trigluon correlation, the two parton composite state is composed of two gluons instead of a quark and gluon as described above for the Qiu-Sterman correlation [11,15]. The collinear factorization framework has been widely used to describe the TSSA's measured at RHIC [16–23].

An alternative treatment is known as the transverse-momentum-dependent (TMD) formalism. In this formalism, the cross section is factorized into hard-scattering cross sections and TMD parton distribution and fragmentation functions (PDFs and FFs) [24]. For the TMD approach to be valid in the context of $p + p$ collisions, Q^2 must be large, in order to use perturbative QCD, while the transverse momentum must satisfy $p_T \ll Q$ and not be much larger than the intrinsic, parton transverse momentum k_T, so that effects of the latter remain visible [25]. One of the TMD PDFs, called the Sivers function [4], is widely used in describing the TSSA's that were observed in different processes [26–30]. The Sivers function, denoted by $f_{1T}^\perp(x, \mathbf{k}_\perp^2)$, describes the distortion in the distribution of

unpolarized partons with momentum fraction x and transverse momentum $\mathbf{k}_\perp$ in a transversely polarized hadron. This distorted distribution of unpolarized partons causes an azimuthal anisotropy in the distribution of parton transverse momenta in the polarized hadron which gives rise to the nonzero TSSA. As it has been described above, at low p_T, the nonperturbative TMD Sivers function will be responsible for its SSA, while twist-3 dominates the contributions to the SSA when $p_T \sim Q$. At intermediate p_T, one can see the transition between these two frameworks and a relation between Sivers function and Qiu-Sterman function has been shown in Ref. [31].

With increasing experimental information on the quark Sivers function during the last ten years, our understanding of this quantity has matured [32–36], while the gluon Sivers function is still relatively unknown. The transversely polarized $p + p$ collisions studied at RHIC present a very good opportunity to study the gluon Sivers function as gluon-gluon interactions are dominant in $p + p$ collisions at RHIC energies. PHENIX has measured the TSSA for J/ψ production at central and forward rapidities [37] and, at small p_T values, where the J/ψ mass becomes the large scale Q in TMD factorization, the result has been compared to a gluon Sivers function derived in the context of the color-evaporation model in [38] and the generalized-parton model in [39].

In proton-nucleus ($p + A$) collisions, the increase of the atomic number results in increasing gluon occupancy, and therefore gluon saturation effects may become important in the small x region. In the Regge-Gribov limit, the properties of saturated gluons in the infinite-momentum frame can be described by the color glass condensate (CGC) which has been applied to a variety of processes such as $e + p$, $e + A$, $A + A$, and $p + A$ collisions [40]. The quark and gluon distribution functions for large nuclei were computed first in Ref. [41] in the weak coupling limit. Using the CGC framework, one can describe the rescatterings of the outgoing parton within the nucleus. In the coherent QCD multiple scattering framework [42], it has been shown that at low p_T the rates of single and double hadron production are highly suppressed and the amount of suppression grows with rapidity and centrality; meanwhile, at high p_T, such nuclear modification effects become less pronounced as we enter the perturbative region in a dilute nuclear medium. For the computation of TSSA's, a hybrid approach has been widely used in photon, γ-jet and dijet production [43–46]. The hybrid approach treats the gluon distribution inside the heavy nucleus in the CGC framework and utilizes the twist-3 formalism for the proton side. The resummation of the power corrections in $p + A$ reactions shifts the nuclear PDF to higher x [42]. The new PHENIX $p + A$ collision data offer the opportunity to quantify how this shift in x affects the twist-3 description of the TSSA's discussed above.
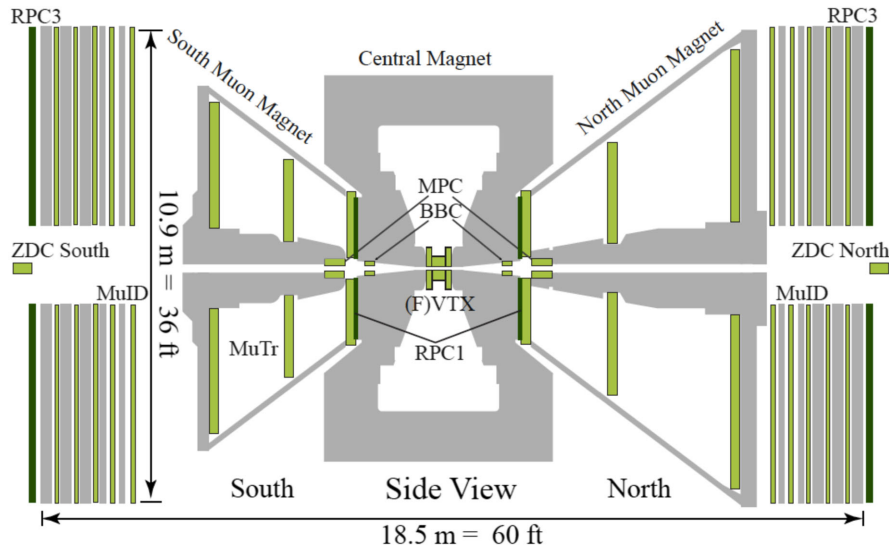
FIG. 1. Side view of the 2015 PHENIX detector. Of primary importance to this analysis are the BBC, MuTr, and MuID. See text for descriptions of these subsystems and how they were used.

II. EXPERIMENT SETUP

The J/ψ mesons are measured by detecting muon pairs $\mu^+\mu^-$ in the two PHENIX muon spectrometers. The two muon spectrometers with full azimuthal coverage cover a range in pseudorapidity $\eta \in [-2.2, -1.2]$ for the south arm and $\eta \in [1.2, 2.4]$ for the north arm (see Fig. 1). The momenta of the muons are measured by the muon trackers (MuTr). The MuTr is composed of three stations of cathode-strip tracking chambers inside a radial magnetic field [47]. The MuTr chambers are followed by the muon identifiers (MuID) which contain five sensitive layers (named gap0–gap4) per arm, with each layer made of one vertically and one horizontally oriented Iarocci tube plane, all interleaved with 10- or 20-cm thick steel absorber plates to suppress hadron backgrounds. With the front absorber provided by the PHENIX central magnets and the MuID together with additional stainless steel absorber mounted in 2011, the total thickness of the steel absorbers is about 190 cm. The probability for a 4 GeV/c pion to punch through the whole absorber is less than 3% [48,49]. Muons with momenta of at least 3 GeV/c can penetrate all the absorbers and reach the last layer of the MuID with high efficiency.

Two beam-beam counters (BBC) are located at opposite ends at 144 cm from the interaction point along the beam line with full azimuthal coverage and $|\eta| \in [3.1, 3.9]$. Each BBC has 64 elements consisting of a quartz Čerenkov radiator and mesh-dynode PMT. The BBCs also serve as an interaction vertex finder with resolution along the beam direction of about 2 cm, and the z-vertex approximately follows a Gaussian distribution centered at 0 with a width of about 10 cm in $p + p$ collisions and in addition play the role of a luminosity detector [50]. For the minimum-bias (MB) trigger, it is required to have one or more hits in each

BBC. The MB-trigger efficiency for $p + p$ collisions is about 55% [51], while this trigger is 84% (72%) efficient for $p + $ Au ($p + $ Al) collisions; the percentage is defined with multiplicity in the south BBC (A-going direction) [52].

Events containing dimuon candidates were selected using the combination of BBC-MB trigger and other muon triggers. The "2-deep muon trigger" requires that both muon tracks have at least one hit in the last two MuID gaps and no less than two hits in other gaps. The "sagitta-3 muon trigger" selects tracks that were recorded by MuTr with high momentum, requiring that the maximum track sagitta, determined by the 3 MuTr stations, be less than 3 MuTr cathode strips at the middle plane.

The dimuon candidates are then screened by the dimuon cuts shown in Table I. Here, p_z and p_T are respectively the longitudinal and transverse momentum of the dimuon pair with respect to the beam direction, the lower-side p_T cut is

TABLE I. Track selections and cuts used in this analysis. See text for definitions and details.

Single muon cuts	DG0 < 30 cm (south)
	DG0 < 25 cm (north)
	DDG0 < 10°
	lastgap > 2
	ntrhits > 9
	nidhits > 5
	MuTr DCA$_r$ < 10 cm
Dimuon cuts	p_z < 100 GeV/c
	0.42 GeV/c < p_T < 10 GeV/c
	$-2.2 < \eta < -1.2$ (south)
	$1.2 < \eta < 2.2$ (north)
	vertex χ^2 < 5
	-30 cm < BBC$_z$ vertex < 30 cm

TABLE II.　Blue and yellow beam polarization in $p + p$ and $p + A$ collisions.

Data set	Blue beam	Yellow beam
$p + p$	57%	57%
$p + Al$	57%	0
$p + Au$	61%	0

imposed due to the MuTr resolution, DG0 is the distance between two matched tracks coming one each from the MuTr and MuID, projected to the first MuID gap, DDG0 is the opening angle between these projected tracks, ntrhits (nidhits) is the number of hits generated by a track in the MuTr (MuID), lastgap is the last-gap number in the MuID that a track penetrates, and DCA$_r$ is the distance of closest approach between a muon track and the beam line. The event vertex determined by the BBC follows a Gaussian distribution centered at 0 with a width of about 40 cm. A z-position vertex cut within ± 30 cm ensures that the collision occurs inside the spectrometer acceptance and keeps approximately 50% of all collisions. The vertex χ^2 is determined by fitting the two candidate tracks with the event vertex given by the BBC.

In the 2015 RHIC run, we took 11 weeks of $p + p$ collision data with an integrated luminosity of about 40 pb^{-1} and with both the blue beam (clockwise) and yellow beam (counterclockwise) transversely (vertically) polarized at the PHENIX interaction point. In $p + A$ collisions, only the blue beam (the proton beam) was polarized; we have 2- and 5-week data sets for $p + Al$ and $p + Au$ with integrated luminosities of about 6.0 pb^{-1} and 6.6 pb^{-1}, respectively. Table II shows the beam polarizations. Each proton beam was filled into 111 bunches with different spin states in eight base patterns [53].

III. DATA ANALYSIS

The maximum likelihood method was used to extract the transverse single spin asymmetry A_N. The likelihood $\mathcal{L}$ for one dimuon pair with azimuthal angle ϕ with respect to the incoming polarized proton beam direction is $1 + P \cdot A_N \sin(\phi_{\text{pol}} - \phi)$, where P is the beam polarization, and ϕ_{pol} is the direction of beam polarization which is $+(-)\pi/2$ when the spin is up (down). Then the log-likelihood for all the dimuon pairs is given by

$$\log \mathcal{L} = \sum_i \log(1 + P \cdot A_N \sin(\phi_{\text{pol}} - \phi_i)). \quad (2)$$

We select the value of A_N that maximizes $\mathcal{L}$. The statistical uncertainty of A_N is obtained by calculating the inverse of the second derivative of $\mathcal{L}$ with respect to A_N,

$$\sigma^2(A_N) = \left(-\frac{\partial^2 \log \mathcal{L}}{\partial A_N^2} \right)^{-1}. \quad (3)$$

To extract the $J/\psi A_N$, first we calculated the inclusive A_N (A_N^{incl}) in the J/ψ invariant mass region between 2.8 GeV/c^2 and 3.4 GeV/c^2. Then we corrected that A_N with the background A_N (A_N^{bgr}) using Eq. (4) and calculated the corresponding uncertainty in $A_N^{J/\psi}$ using Eq. (5),

$$A_N^{J/\psi} = \frac{A_N^{\text{incl}} - f \cdot A_N^{\text{bgr}}}{1 - f} \quad (4)$$

$$\delta A_N^{J/\psi} = \frac{\sqrt{(\delta A_N^{\text{incl}})^2 + f^2 \cdot (\delta A_N^{\text{bgr}})^2}}{1 - f}. \quad (5)$$
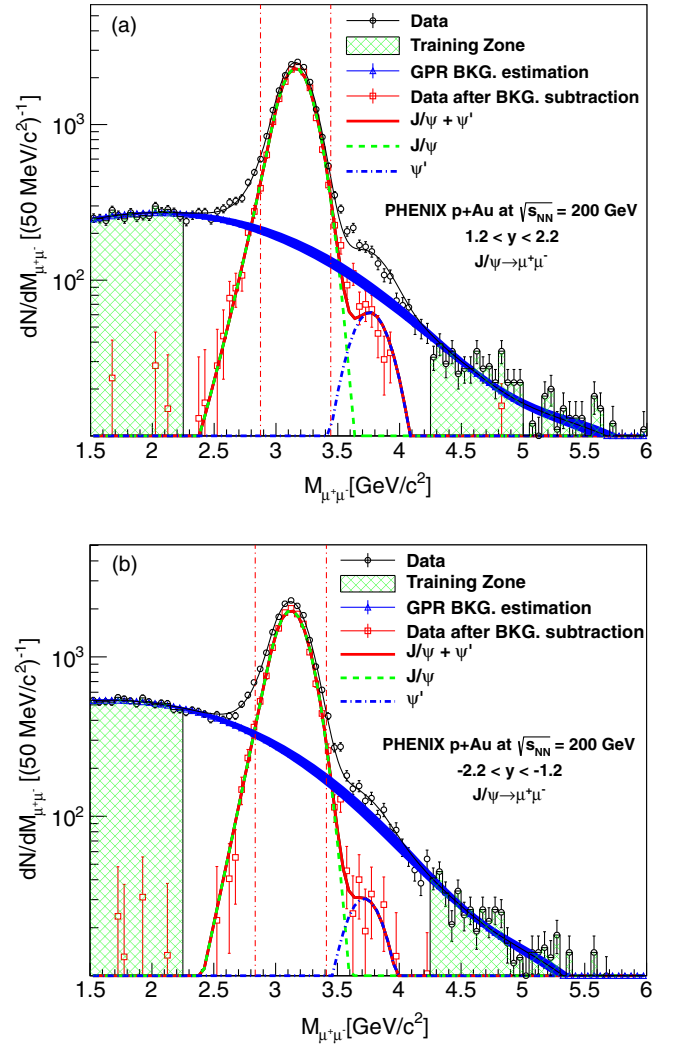

FIG. 2.　Dimuon mass spectrum fits with GPR background estimation for $0.42 < p_T < 10$ GeV/c for the (a) p-going and (b) Au-going directions.
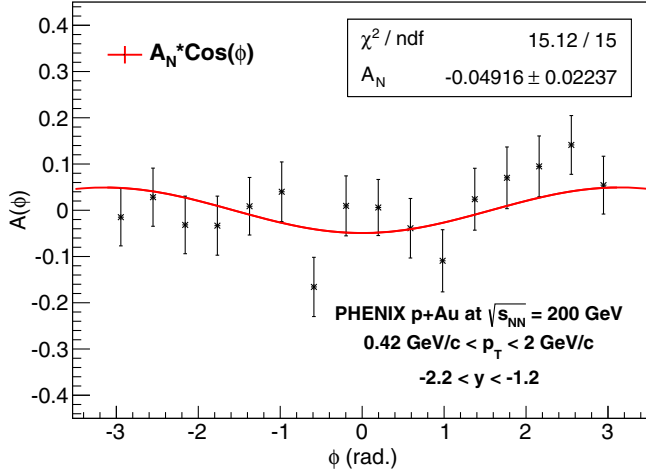
FIG. 3. Fit of inclusive $A(\phi)$ with a cosine modulation. The asymmetry and χ^2 per degree of freedom from the fit are shown.

Here, f is the background fraction in the J/ψ invariant mass region. The statistical uncertainty from f is not taken into account because its contribution to the total statistical uncertainty is small ($< 5\%$).

The background A_N under the J/ψ peak was estimated from a sideband in the dimuon invariant mass range of 1.5–2.4 GeV/c^2; a similar approach was used in previous PHENIX measurements [54,55]. The background fraction f was obtained using the Gaussian process regression (GPR) method [56–59] for each p_T and x_F bin. The GPR method is a nonparametric regression approach considered to be less biased and has been used in several previous PHENIX measurements [55,60]. Figure 2 shows the fitting result with the GPR method using $p + $Au data. The dimuon invariant mass windows of 1.5 GeV/c^2 to 2.2 GeV/c^2 and 4.3 GeV/c^2 to

6.0 GeV/c^2 are used for estimating the background shape (see Fig. 2). Then the signal [J/ψ and $\psi(2S)$] yields are obtained by subtracting the GPR background from the inclusive dimuon spectrum. The J/ψ and $\psi(2S)$ peaks are fitted respectively by a crystal ball function [61] and a Gaussian function. The vertical lines in Fig. 2 represent $\pm 2\sigma$ mass windows around the J/ψ peak, where the $\psi(2S)$ contribution will be negligible; J/ψ production is dominant in both the p-going and Au-going directions. The background fraction is 17% for the Au-going direction, 13% for the Al-going direction and 10% for the p-going direction.

The A_N^{incl} and A_N^{bgr} asymmetries for each p_T and x_F bin are calculated with the maximum likelihood method described above but with different dimuon invariant mass windows. For A_N^{incl} we used unlike-sign muon pairs in the invariant mass range $\pm 2\sigma$ around the J/ψ peak, while for A_N^{bgr} we used the fixed invariant mass range from 1.5 GeV/c^2 to 2.4 GeV/c^2.

In this analysis, there are two sources of systematic uncertainty, detailed as sources 1 and 2 in the following two paragraphs and listed quantitatively in Tables III and IV. For the total systematic uncertainty displayed in Figs. 4 and 5, we have combined these two sources quadratically.

The first systematic uncertainty source ("source 1") concerns the method of determining the asymmetry itself. We check this by determining A_N with a different method, the azimuthal fitting method. Similar to Eq. (2), the production cross section of J/ψ as a function of the azimuthal angle ϕ is given by

$$\sigma(\phi) \propto 1 + P \cdot A_N \sin(\phi_{\text{pol}} - \phi), \qquad (6)$$

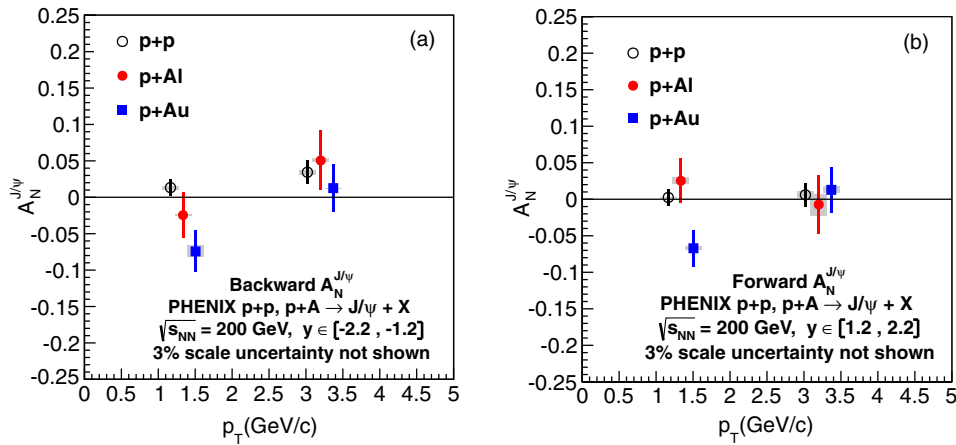where $\phi_{\text{pol}} = +(-)\pi/2$ when the spin is up (down).

FIG. 4. (a) Backward [$x_F < 0$] and (b) forward [$x_F > 0$] $A_N^{J/\psi}$ vs p_T for open [black] circles $p + p$, closed [red] circles $p + $Al, and closed [blue] boxes $p + $Au collisions. The shaded [gray] boxes show the systematic uncertainty. The data points for $p + $Al and $p + $Au collisions have been shifted in p_T for clarity.

TABLE III. $A_N^{J/\psi}$ for ranges of p_T in forward and backward rapidity for $p+p$, $p+$Al, and $p+$Au collisions.

Range of x_F	p_T(GeV/c)	Data sample	$\langle p_T\rangle$(GeV/c)	A_N	δA_N^{stat}	δA_N^{syst}(source 1)	δA_N^{syst}(source 2)
Forward ($x_F>0$)	$0.42 < p_T < 2$	$p+p$	1.17	0.002	0.011	0.0006	0.0001
		$p+$Al	1.19	0.025	0.030	0.0034	0.0026
		$p+$Au	1.20	−0.067	0.025	0.0008	0.0020
	$2 < p_T < 10$	$p+p$	3.02	0.006	0.016	0.0009	0.0041
		$p+$Al	3.07	−0.007	0.040	0.0148	0.0005
		$p+$Au	3.13	0.013	0.031	0.0045	0.0015
Backward ($x_F<0$)	$0.42 < p_T < 2$	$p+p$	1.16	0.013	0.011	0.0021	0.0002
		$p+$Al	1.18	−0.024	0.031	0.0007	0.0012
		$p+$Au	1.19	−0.074	0.029	0.0077	0.0008
	$2 < p_T < 10$	$p+p$	3.00	0.034	0.016	0.0027	0.0015
		$p+$Al	3.03	0.050	0.041	0.0024	0.0001
		$p+$Au	3.03	0.013	0.033	0.0004	0.0004

The asymmetry can be written as function of azimuthal angle ϕ as

$$A(\phi) = \frac{\sigma^\uparrow(\phi) - \sigma^\downarrow(\phi)}{\sigma^\uparrow(\phi) + \sigma^\downarrow(\phi)} = A_N \cdot \cos(\phi). \qquad (7)$$

Therefore, A_N can be extracted by fitting the $A(\phi)$ with a cosine modulation. As an example, Fig. 3 shows the determination of A_N^{incl} for dimuons with $0.42 < p_T < 2$ GeV/c in the Au-going direction. The differences of $J/\psi A_N$ determined from the maximum likelihood method and azimuthal fitting method are treated as a systematic uncertainty. The value of the source 1 uncertainty ranges from 1% to 35% of the statistical uncertainties.

A second source of systematic uncertainty ("source 2") is from the method of determining the background fraction f. We studied a potential bias of the GPR method by parameterizing the background with a third order polynomial instead. The f changed by about 2%, and the corresponding difference in the resulting background corrected $J/\psi A_N$s has been assigned as a systematic uncertainty which is of the order of 10% of the statistical uncertainty.

IV. RESULTS

Figure 4 and Table III show the TSSA for J/ψ production, $A_N^{J/\psi}$, in two p_T bins in forward and backward kinematics in $p+p$, $p+$Al and $p+$Au collisions. The 2015 $p+p$ data are consistent with the previous results of $A_N^{J/\psi}$ from the 2006 and 2008 data [37] within one-standard-deviation. The 2015 $p+p$ data favor a positive asymmetry (at the 2σ level) in the high-p_T bin in backward rapidity. With limited statistics, the A_N in all p_T and x_F bins for $p+$Al collisions are consistent with zero. In $p+$Au

collisions, the asymmetry in the high-p_T bin is consistent with zero, although there is a trend to a nonzero A_N (at the 2σ level) in the low-p_T bin in both the forward and backward directions.

Figure 5 and Table IV show the $A_N^{J/\psi}$ as a function of x_F. In the $p+p$ data, it is consistent with the previous PHENIX results [37] and a $\sim 2\sigma$ positive A_N is observed in the backward higher x_F bin. The result for the other x_F bins are consistent with zero. For the $p+$Au data, a $\sim 2\sigma$ negative A_N is observed in the forward high-x_F bin and the backward low-x_F bin. A scale uncertainty from the polarization (3%) is not included in both Figs. 4 and 5.
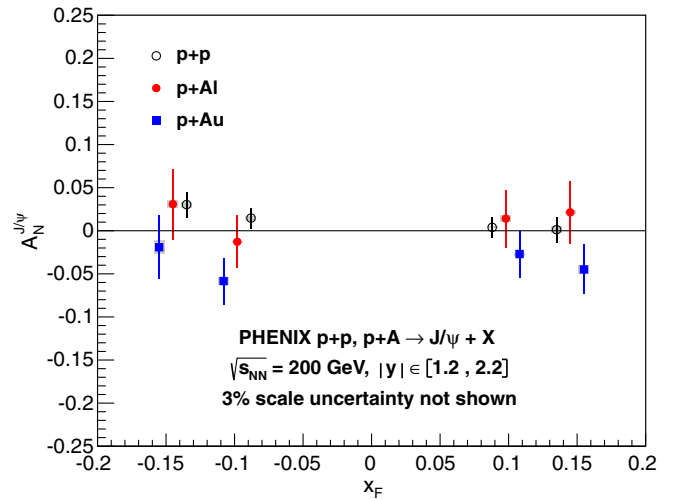

FIG. 5. $A_N^{J/\psi}$ vs x_F for open [black] circles $p+p$, closed [red] circles $p+$Al, and closed [blue] boxes $p+$Au collisions. The shaded [gray] boxes show the systematic uncertainty. The data points for $p+$Al and $p+$Au collisions have been shifted in x_f for clarity.

TABLE IV. $A_N^{J/\psi}$ for ranges of x_F in forward and backward rapidity for $p + p$, $p + \text{Al}$ and $p + \text{Au}$ collisions.

Range of x_F	Data sample	$\langle x_F \rangle$	A_N	δA_N^{stat}	δA_N^{syst}(source 1)	δA_N^{syst}(source 2)
$0.05 < x_F < 0.11$	$p + p$	0.088	0.004	0.012	0.0001	0.0006
	$p + \text{Al}$	0.089	0.014	0.033	0.0029	0.0021
	$p + \text{Au}$	0.089	−0.027	0.027	0.0014	0.0001
$0.11 < x_F < 0.30$	$p + p$	0.135	0.001	0.015	0.0018	0.0030
	$p + \text{Al}$	0.135	0.021	0.036	0.0011	0.0013
	$p + \text{Au}$	0.136	−0.045	0.029	0.0049	0.0003
$-0.11 < x_F < -0.05$	$p + p$	−0.086	0.013	0.012	0.0026	0.0002
	$p + \text{Al}$	−0.086	−0.013	0.030	0.0007	0.0004
	$p + \text{Au}$	−0.086	−0.058	0.027	0.0040	0.0007
$-0.30 < x_F < -0.11$	$p + p$	−0.132	0.030	0.015	0.0031	0.0011
	$p + \text{Al}$	−0.132	0.031	0.041	0.0002	0.0041
	$p + \text{Au}$	−0.132	−0.019	0.037	0.0077	0.0006

V. CONCLUSION

We have reported the measurements of the transverse single-spin asymmetry in J/ψ production at forward and backward rapidity with $1.2 < |y| < 2.2$ in $p + p$, $p + \text{Al}$ and $p + \text{Au}$ collisions with transversely polarized proton beams at $\sqrt{s_{NN}} = 200$ GeV using the RHIC run 2015 data. The results from $p + p$ collisions are consistent with previous PHENIX results. Within experimental uncertainties, the $J/\psi A_N$ is consistent with zero in all p_T and x_F bins in $p + \text{Al}$ collisions. For $p + \text{Au}$ collisions, the data favor negative asymmetries in all x_F bins, and we have observed a nonzero A_N at the 2σ level in the lower-p_T bins; however, in the higher-p_T bins, it is consistent with zero. This intriguing result observed in $p + \text{Au}$ collisions could indicate possible contributions from other nonconventional mechanisms. One of the possible contributions could come from electromagnetic interactions. A recent PHENIX measurement [62] of the TSSA in forward neutron production shows that electromagnetic processes could significantly enhance A_N in $p + A$ collisions, resulting in a strong nuclear-size dependence for A_N. Further theoretical studies of A_N in J/ψ production exploring different mechanisms are needed to explain the current results.

ACKNOWLEDGMENTS

[1] G. L. Kane, J. Pumplin, and W. Repko, Transverse Quark Polarization in Large p(T) Reactions, e+ e- Jets, and Leptoproduction: A Test of QCD, Phys. Rev. Lett. **41,** 1689 (1978).

[2] R. D. Klem, J. E. Bowers, H. W. Courant, H. Kagan, M. L. Marshak, E. A. Peterson, K. Ruddick, W. H. Dragoset, and J. B. Roberts, Measurement of Asymmetries of Inclusive Pion Production in Proton-Proton Interactions at 6-GeV/c and 11.8-GeV/c, Phys. Rev. Lett. **36,** 929 (1976).

[3] E.-C. Aschenauer *et al.*, The RHIC SPIN program: Achievements and future opportunities, arXiv:1501.01220.

[4] D. W. Sivers, Single spin production asymmetries from the hard scattering of point-like constituents, Phys. Rev. D **41,** 83 (1990).

[5] D. W. Sivers, Hard scattering scaling laws for single spin production asymmetries, Phys. Rev. D **43,** 261 (1991).

[6] J. C. Collins, Fragmentation of transversely polarized quarks probed in transverse momentum distributions, Nucl. Phys. **B396,** 161 (1993).

[7] A. V. Efremov and O. V. Teryaev, QCD asymmetry and polarized hadron structure functions, Phys. Lett. **150B,** 383 (1985).

[8] J.-W. Qiu and G. F. Sterman, Single Transverse Spin Asymmetries, Phys. Rev. Lett. **67,** 2264 (1991).

[9] J.-W. Qiu and G. F. Sterman, Single transverse spin asymmetries in direct photon production, Nucl. Phys. **B378,** 52 (1992).

[10] Z.-B. Kang, F. Yuan, and J. Zhou, Twist-three fragmentation function contribution to the single spin asymmetry in p p collisions, Phys. Lett. B **691,** 243 (2010).

[11] Z.-B. Kang and J.-W. Qiu, Evolution of twist-3 multi-parton correlation functions relevant to single transverse-spin asymmetry, Phys. Rev. D **79,** 016003 (2009).

[12] Z.-B. Kang and J.-W. Qiu, Single transverse-spin asymmetry for D-meson production in semi-inclusive deep inelastic scattering, Phys. Rev. D **78,** 034005 (2008).

[13] J. Qiu and G. Sterman, Single transverse-spin asymmetries in hadronic pion production, Phys. Rev. D **59,** 014004 (1998).

[14] Z.-B. Kang, J.-W. Qiu, and H. Zhang, Quark-gluon correlation functions relevant to single transverse spin asymmetries, Phys. Rev. D **81,** 114030 (2010).

[15] V. M. Braun, A. N. Manashov, and B. Pirnay, Scale dependence of twist-three contributions to single spin asymmetries, Phys. Rev. D **80,** 114002 (2009); Erratum **86,** 119902 (2012).

[16] J. Adams *et al.* (STAR Collaboration), Cross Sections and Transverse Single Spin Asymmetries in Forward Neutral Pion Production from Proton Collisions at $\sqrt{s} = 200$ GeV, Phys. Rev. Lett. **92,** 171801 (2004).

[17] B. I. Abelev *et al.* (STAR Collaboration), Forward Neutral Pion Transverse Single Spin Asymmetries in $p + p$ Collisions at $\sqrt{s} = 200$ GeV, Phys. Rev. Lett. **101,** 222001 (2008).

[18] L. Adamczyk *et al.* (STAR Collaboration), Transverse single-spin asymmetry and cross-section for π^0 and η mesons at large Feynman-x in polarized $p + p$ collisions at $\sqrt{s} = 200$ GeV, Phys. Rev. D **86,** 051101 (2012).

[19] S. S. Adler *et al.* (PHENIX Collaboration), Measurement of Transverse Single-Spin Asymmetries for Midrapidity Production of Neutral Pions and Charged Hadrons in Polarized $p + p$ Collisions at $\sqrt{s} = 200$ GeV, Phys. Rev. Lett. **95,** 202001 (2005).

[20] A. Adare *et al.* (PHENIX Collaboration), Cross section and transverse single-spin asymmetry of η mesons in $p^\uparrow + p$ collisions at $\sqrt{s} = 200$ GeV at forward rapidity, Phys. Rev. D **90,** 072008 (2014).

[21] A. Adare *et al.* (PHENIX Collaboration), Measurement of transverse-single-spin asymmetries for midrapidity and forward-rapidity production of hadrons in polarized $p + p$ collisions at $\sqrt{s} = 200$ and 62.4 GeV, Phys. Rev. D **90,** 012006 (2014).

[22] C. Aidala *et al.* (PHENIX Collaboration), Cross section and transverse single-spin asymmetry of muons from open heavy-flavor decays in polarized $p + p$ collisions at $\sqrt{s} = 200$ GeV, Phys. Rev. D **95,** 112001 (2017).

[23] I. Arsene *et al.* (BRAHMS Collaboration), Single Transverse Spin Asymmetries of Identified Charged Hadrons in Polarized $p + p$ Collisions at $\sqrt{s} = 62.4$ GeV, Phys. Rev. Lett. **101,** 042001 (2008).

[24] M. Anselmino, M. Boglione, U. D'Alesio, E. Leader, S. Melis, F. Murgia, and A. Prokudin, On the role of Collins effect in the single spin asymmetry A_N in $p^\uparrow p \to hX$ processes, Phys. Rev. D **86,** 074032 (2012).

[25] J. C. Collins, D. E. Soper, and G. F. Sterman, Transverse momentum distribution in Drell-Yan pair and W and Z boson production, Nucl. Phys. **B250,** 199 (1985).

[26] A. Airapetian *et al.* (HERMES Collaboration), Single-Spin Asymmetries in Semi-Inclusive Deep-Inelastic Scattering on a Transversely Polarized Hydrogen Target, Phys. Rev. Lett. **94,** 012002 (2005).

[27] C. Adolph *et al.* (COMPASS Collaboration), First measurement of the Sivers asymmetry for gluons using SIDIS data, Phys. Lett. B **772,** 854 (2017).

[28] R. M. Godbole, A. Kaushik, A. Misra, V. Rawoot, and B. Sonawane, Heavy flavour production as probe of gluon Sivers function, Few-Body Syst. **58,** 96 (2017).

[29] U. D'Alesio, F. Murgia, and C. Pisano, Towards a first estimate of the gluon Sivers function from A_N data in pp collisions at RHIC, J. High Energy Phys. 09 (2015) 119.

[30] A. Mukherjee and S. Rajesh, J/ψ production in polarized and unpolarized ep collision and Sivers and $\cos 2\phi$ asymmetries, Eur. Phys. J. C **77,** 854 (2017).

[31] D. Boer, P. J. Mulders, and F. Pijlman, Universality of T-odd effects in single spin and azimuthal asymmetries, Nucl. Phys. **B667,** 201 (2003).

[32] M. Anselmino, M. Boglione, U. D'Alesio, S. Melis, F. Murgia, and A. Prokudin, Sivers effect and the single spin asymmetry A_N in $p^\uparrow p \to hX$ processes, Phys. Rev. D **88,** 054023 (2013).

[33] M. Anselmino, M. Boglione, U. D'Alesio, A. Kotzinian, S. Melis, F. Murgia, A. Prokudin, and C. Turk, Sivers effect for pion and kaon production in semi-inclusive deep inelastic scattering, Eur. Phys. J. A **39,** 89 (2009).

[34] J. C. Collins, A. V. Efremov, K. Goeke, S. Menzel, A. Metz, and P. Schweitzer, Sivers effect in semi-inclusive deeply inelastic scattering, Phys. Rev. D **73,** 014021 (2006).

[35] W. Vogelsang and F. Yuan, Single-transverse spin asymmetries: From DIS to hadronic collisions, Phys. Rev. D **72,** 054028 (2005).

[36] M. Anselmino, M. Boglione, U. D'Alesio, A. Kotzinian, F. Murgia, and A. Prokudin, Extracting the Sivers function from polarized SIDIS data and making predictions, Phys. Rev. D **72,** 094007 (2005); Erratum **72,** 099903 (2005).

[37] A. Adare *et al.* (PHENIX Collaboration), Measurement of transverse single-spin asymmetries for J/ψ production in polarized $p + p$ collisions at $\sqrt{s} = 200$ GeV, Phys. Rev. D **82,** 112008 (2010); Erratum **86,** 099904 (2012).

[38] R. M. Godbole, A. Kaushik, A. Misra, V. Rawoot, and B. Sonawane, Transverse single spin asymmetry in $p + p^{\uparrow} \rightarrow J/\psi + X$, Phys. Rev. D **96,** 096025 (2017).

[39] U. D'Alesio, F. Murgia, C. Pisano, and P. Taels, Probing the gluon Sivers function in $p^{\uparrow}p \rightarrow J/\psi X$ and $p^{\uparrow}p \rightarrow DX$, Phys. Rev. D **96,** 036011 (2017).

[40] F. Gelis, E. Iancu, J. Jalilian-Marian, and R. Venugopalan, The color glass condensate, Annu. Rev. Nucl. Part. Sci. **60,** 463 (2010).

[41] L. D. McLerran and R. Venugopalan, Computing quark and gluon distribution functions for very large nuclei, Phys. Rev. D **49,** 2233 (1994).

[42] J. Qiu and I. Vitev, Coherent QCD multiple scattering in proton-nucleus collisions, Phys. Lett. B **632,** 507 (2006).

[43] A. Schäfer and J. Zhou, Transverse single spin asymmetry in direct photon production in polarized pA collisions, Phys. Rev. D **90,** 034016 (2014).

[44] A. Schäfer and J. Zhou, Color entanglement for γ-jet production in polarized pA collisions, Phys. Rev. D **90,** 094012 (2014).

[45] J. Zhou, Single spin asymmetries in forward p-p/A collisions revisited: The role of color entanglement, Phys. Rev. D **96,** 034027 (2017).

[46] J. Zhou, Color entanglement like effect in collinear twist-3 factorization, Phys. Rev. D **96,** 114001 (2017).

[47] H. Akikawa *et al.* (PHENIX Collaboration), PHENIX muon arms, Nucl. Instrum. Methods Phys. Res., Sect. A **499,** 537 (2003).

[48] K. Adcox *et al.* (PHENIX Collaboration), PHENIX detector overview, Nucl. Instrum. Methods Phys. Res., Sect. A **499,** 469 (2003).

[49] S. Adachi *et al.*, Trigger electronics upgrade of PHENIX muon tracker, Nucl. Instrum. Methods Phys. Res., Sect. A **703,** 114 (2013).

[50] K. Adcox *et al.* (PHENIX Collaboration), PHENIX detector overview, Nucl. Instrum. Methods Phys. Res., Sect. A **499,** 469 (2003).

[51] S. S. Adler *et al.* (PHENIX Collaboration), Midrapidity Neutral Pion Production in Proton-Proton Collisions at $\sqrt{s} = 200$ GeV, Phys. Rev. Lett. **91,** 241803 (2003).

[52] A. Adare *et al.* (PHENIX Collaboration), Centrality categorization for $R_{p(d)+A}$ in high-energy collisions, Phys. Rev. C **90,** 034902 (2014).

[53] I. Alekseev, in Configuration Manual: Polarized Proton Collider at RHIC, Technical Report (Brookhaven National Laboratory, Upton, NY, 2006), https://www.bnl.gov/cad/accelerator/docs/pdf/RHICPPCMan.pdf.

[54] A. Adare *et al.* (PHENIX Collaboration), Inclusive cross section and double-helicity asymmetry for π^0 production at midrapidity in $p + p$ collisions at $\sqrt{s} = 510$ GeV, Phys. Rev. D **93,** 011501 (2016).

[55] A. Adare *et al.* (PHENIX Collaboration), Measurements of double-helicity asymmetries in inclusive J/ψ production in longitudinally polarized $p + p$ collisions at $\sqrt{s} = 510$ GeV, Phys. Rev. D **94,** 112008 (2016).

[56] D. J. MacKay, *Information Theory, Inference and Learning Algorithms* (Cambridge University Press, Cambridge, England, 2003).

[57] C. E. Rasmussen and C. K. I. Williams, in *Gaussian Processes for Machine Learning*, edited by T. Dietterich (MIT Press, Cambridge, MA, 2006).

[58] S. L. Lauritzen, *Graphical Models* (Clarendon Press Oxford University Press, Oxford, 1996).

[59] D. Barber, *Bayesian Reasoning and Machine Learning* (Cambridge University Press, Cambridge, England, 2012).

[60] A. Adare *et al.* (PHENIX Collaboration), Measurement of parity-violating spin asymmetries in $W^{\pm}$ production at midrapidity in longitudinally polarized $p + p$ collisions, Phys. Rev. D **93,** 051103 (2016).

[61] T. Skwarnicki, A study of the radiative CASCADE transitions between the Upsilon-Prime and Upsilon resonances, Ph.D. thesis, Cracow, INP, 1986.

[62] C. Aidala *et al.* (PHENIX Collaboration), Nuclear Dependence of the Transverse-Single-Spin Asymmetry for Forward Neutron Production in Polarized $p + A$ Collisions at $\sqrt{s_{NN}} = 200$ GeV, Phys. Rev. Lett. **120,** 022001 (2018).